January 2015

Effects Of Degradation On Mechanical Properties Of Tissue-Engineering Poly(glycolic Acid) Scaffolds

Yushane Celestine Shih
Yale School of Medicine, celestine.shih@gmail.com

Follow this and additional works at: http://elischolar.library.yale.edu/ymtdl

Effects of Degradation on Mechanical Properties of

Tissue-Engineering Poly(glycolic acid) Scaffolds

A Thesis Submitted to

Yale University School of Medicine

In Partial Fulfillment of the Requirements for the

Degree of Doctor of Medicine

by

Yushane Celestine Shih

2015

Thesis Advisor:

Dr. Jay. D. Humphrey, Dept. of Biomedical Engineering

Thesis Committee:

Dr. Tarek Fahmy, Depts. of Biomedical Engineering and Immunobiology

Dr. Themis R. Kyrakides, Depts. of Pathology and Biomedical Engineering

Dr. Laura E. Niklason, Depts. of Anesthiology and Biomedical Engineering

Abstract

EFFECTS OF DEGRADATION ON MECHANICAL PROPERTIES OF TISSUE-ENGINEERING POLY(GLYCOLIC ACID) SCAFFOLDS

Y.C. Shih[1] and J.D. Humphrey[2]

[1] Yale School of Medicine, New Haven, CT
[2] Yale School of Engineering and Applied Sciences, New Haven, CT

Tissue-engineered vascular grafts (TEVGs) offer tremendous therapeutic potential for congenital cardiovascular malformations, and our computational model of growth and remodeling may help expedite TEVG design by identifying optimal scaffold parameters. To evaluate our model's assumptions about scaffold physical properties, we measured the effects of *in vitro* hydrolytic degradation on the compressibility and mechanical behavior of poly(glycolic acid) (PGA) scaffolds. Degradation in neutral PBS at 37°C passed through two stages of first-order decay: the first 50 percent of PGA mass was lost from 5 to 40 days (~1 to 6 weeks) at a rate constant of 0.175 wk^{-1}, after which the mass degraded with a rate constant of 0.091 wk^{-1}. The half-life of PGA coincided with a drop in the rate of pH change from 2.5 wk^{-1} to 1.5 wk^{-1} at 6 weeks, showing that the remaining mass of polymer influences the creation of acidic degradation byproducts from PGA. Over 25 days, the degrading scaffolds became less stiff (Young's modulus decreased from 6.45 to 0.12 MPa), underwent a dissipative, non-elastic process during repeated loading-unloading cycles, and exhibited increasing diversity of mechanical behavior that is similar to the phenotypic diversity manifested by 2 year-old TEVG grafts [2]. Incompressibility was maintained until day 25, possibly because by then the scaffolds are heterogeneously fragmented and the load is not transmitted evenly throughout the material. These scaffolds behave in a complex manner as they degrade *in vitro*, and more complete data are necessary to inform the next generation of computational models and to illustrate clearly the evolving mechanical behavior of TEVGs from implantation to neovessel formation.

Acknowledgements

Table of Contents

Background & Clinical Significance

Tissue engineered vascular grafts (**TEVGs**) offer significant promise to cardiovascular medicine as evidenced by the first successful human clinical trial over 10 years ago, which used TEVGs to treat children with congenital heart defects [3]. Yet, development of this technology remains hindered by the time-consuming "trial and error" approach of tissue engineering, and stenosis remains a complication.

Congenital cardiovascular malformations are the most common cause of infant death due to birth defects [4]. They represent a heavy burden in terms of morbidity, mortality, and healthcare costs; nearly 40,000 births per year in the United States are affected by congenital heart defects, and 25 percent of these children have a critical defect that generally requires surgery or other procedures during their first year of life [5-7]. Surgical management has improved greatly, but is not without risk of complications: thrombo-embolic events, infection, and poor durability due to neointimal hyperplasia or ectopic calcification [8]. Because the synthetic devices utilized in most reconstructive operations lack growth potential, children may require replacement surgeries as they outgrow their implants, which substantially increases overall morbidity and mortality [8].

Scaffolds for tissue engineering, in contrast, resorb once they have served their purpose as a template for vascular regeneration. Tissue engineering aims to restore or replace defective tissue by creating biological substitutes; a polymeric scaffold provides initial structural support and biological and physical cues for tissue development, thus mimicking the functions of endogenous extracellular matrix (ECM). As the scaffold degrades, neotissue forms in its place [9]. *The greatest advantage of TEVGs is their*

potential to grow and develop with the child. In the most recent follow-up of the first clinical trial of TEVGs implanted as conduits from the inferior vena cava (IVC) to the pulmonary artery, 25 children demonstrated low risk for thromboembolic events – the most common complication associated with synthetic grafts – and no signs of graft-related mortality or aneurysmal dilation, graft rupture, or graft infection [10] (**Figure 1**). The primary mode of graft failure was stenosis in four patients who were successfully treated by balloon angioplasty. Clinical experience thus far affirms the overall safety and efficacy of our TEVGs compared with current synthetic grafts, and most importantly, their growth potential.

Figure 1: CT scan of a TEVG implanted in a child, connecting the IVC to the pulmonary artery, three years post-implantation (modified Fontan procedure for congenital single ventricle physiology). Note that there is no dilation or stenosis [1].

Although the clinical utility of TEVGs is promising, little is known about how these polymeric constructs transform into living blood vessels in host recipients. Our findings

have suggested that circulating host monocytes release myriad inflammatory cytokines and growth factors, recruiting macrophages and cells from the surrounding native vessel and perivascular tissue to migrate into the polymer scaffold [11, 12]. This inflammatory response will dictate the graft's success or failure, and the scaffold's material characteristics – chemical, physical, and morphological – play an important role in modulating cellular events and their path towards normal or pathological wound healing [13]. For example, hydrophilic surface chemistries decrease *in vivo* expression of inflammatory cytokines by surrounding immune cells [14]. Macrophages, the most important component of innate immunity, may shift to a pro-inflammatory (M1) or pro-healing (M2) subtype depending on the surface micro-pattern, material morphology, fiber diameter, and pore size [14-17]. Fibroblasts preserve collagen homeostasis by sensing mechanical stimuli and changing their phenotype accordingly; exposure to a substrate that is stiffer than their physiological environment will activate a myofibroblast phenotype that simultaneously exhibits contractile activity and high matrix secretion [18, 19]. Many other physico-chemical properties also influence tissue remodeling (see **Table 1** for more examples), but understanding the full extent of their effects remains a challenge, particularly when scaffold degradation enters the picture.

As the primary immunological stimulus and initial source of structural integrity, the scaffold determines multiple aspects in the growth and remodeling process, and it is crucial that we understand how these change as the polymer degrades. The poly(glycolic acid), or PGA, polymer used in our venous TEVG scaffolds has been approved for biodegradable medical devices since the late 1970s, but reports on its degradation profile are inconsistent [20]. There are some reports that monofilaments of PGA can be degraded

in as little as two to four weeks [21], whereas others report that PGA sutures are not completely resorbed until about four months although they lose 70 percent of their mechanical strength within two weeks of implantation [20]. In our own venous grafts, Naito and colleagues reported that half of the PGA volume was lost when explanted at two weeks, and nearly no scaffold was detected at 12 weeks when measured with polarized light or Masson's trichrome staining [22]. What happens to the polymeric scaffold during the interval between those time points is unknown. This gap in our knowledge – as well as the inconsistency in literature - calls for further investigation about scaffold degradation and its involvement in the changing macroscopic behavior of engineered veins.

	SCAFFOLD	NEOVESSEL
Scaffold Property	**Inflammation-Mediated**	**Stress-Mediated**
Mass	Foreign body response	Stress-shielding
Hydrophobicity	Protein adhesion	Mass loss
Porosity, Pore size	Cell infiltration Macrophage phenotype	Degradation Scaffold mechanics
Surface roughness	Cell/protein adhesion	Fragmentation Scaffold mechanics
pH of degradation byproducts ($\uparrow$ acidity)	$\downarrow$ cell migration De-differentiation	Autocatalysis = More degradation
Compressibility, Isotropy, Stiffness	Fibroblast phenotype	Mechanotransduction
Fiber diameter ($\uparrow$ diameter)	Pro-inflammatory cytokines Foreign body giant cells Angiogenic cytokines	Stiffness

Table 1: Select scaffold physico-chemical properties are listed above after an extensive literature search for primary drivers of vascular growth and remodeling [13, 16-18, 23-26]. The early phase of extracellular matrix production is dominated by inflammation, and

as the scaffold degrades and gives rise to neotissue, it is thought that the cells transition to mechano-sensing and secrete and remodel matrix in response to mechanical stresses [27].

Using computational modeling, it is possible to predict macroscopic mechanical properties of the scaffold based on microscopic design parameters. Predictions obtained by a good mathematical model can provide valuable insight into optimal properties of the scaffold. That is, by comparing predictions with experimental findings, we can better identify contributions of individual constituents to the overall mechanical behavior of the scaffold. Whereas current endeavors in tissue engineering mainly occur by "trial and error" experimentation, time-efficient parametric studies enable a rational approach to designing TEVGs. Reducing the experimental search space with input from computational models may help advance our search for optimal combinations of scaffold structure and material properties [10, 28, 29]. Yet, such computational models must be informed by reliable data, and there is currently scant information in the literature on the biomechanical behavior of a degrading polymer scaffold. O'Dea and colleagues used a multiphase continuum framework to study the interplay between *in vitro* tissue growth and scaffold degradation, albeit within the limited settings of a fspecially designed perfusion bioreactor [30]. Soares and Moore, and later Vieira and colleagues, proposed a neo-Hookean model that reasonably approximates, but does not accurately simulate, how the polymer responds at each stage of degradation [31, 32].

Novel innovations by our group have paved the way for creating second-generation computational models and TEVGs with improved functionality: electrospinning

techniques for fabricating scaffolds having different mechanical and structural properties [11, 33] enable model suggested physical parameters to be tested experimentally; a miniaturized TEVG for *in vivo* studies in diverse transgenic murine models [33] enables detailed longitudinal studies to test graft efficacy; a custom computer-controlled biaxial testing system, designed specifically for testing mouse vessels, enables us to collect novel biomechanical data on the evolution of TEVG properties (**Figure 2A**); and, development of a first-generation computational model for TEVGs that accounts for polymer degradation kinetics and the synthesis and degradation of primary structural components enables data-driven, time-efficient parametric studies (**Figure 2B**) [22, 28, 34-36]. Capitalizing on these advances, one of our primary goals is to understand neovessel formation as a sequence of inflammation-mediated followed by mechanobiological processes involving host cells that result in a replacement conduit having near native properties, including growth potential [11, 12]. Toward this end, biomechanical properties of patent versus stenotic inferior vena cava (IVC) interposition grafts were quantified in two murine models – wild type (C-17) and immunodeficient-beige (SCID-bg) – which exhibit significantly different rates of TEVG stenosis [10, 22]. Using these data, we then extended a prior growth and remodeling computational model for native vessels to incorporate the monotonic loss of load bearing capability by the polymeric scaffold, the inflammation- and mechano-mediated production of collagen, and the evolution of collagen properties after deposition [36].
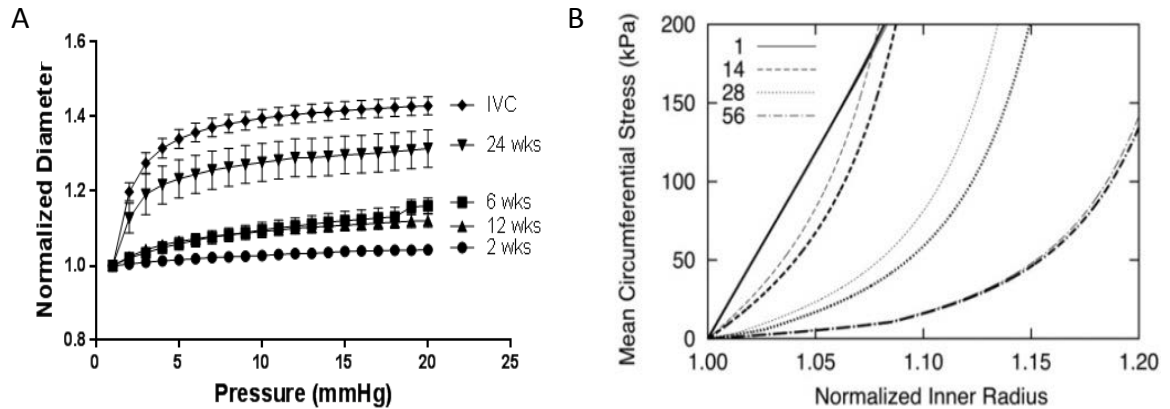
Figure 2: (A) Measured pressure-diameter curve for actual TEVGs over 6 months of implantation; note its similarity to IVC compliance by 24 weeks [22]. (B) Predicted changes in circumferential wall mechanics over time for a collagenous TEVG [18].

This extended model depicts many of the salient mechanical features of an evolving TEVG, but it is only a first-generation model, and many of its assumptions need to be evaluated with more complete data – in particular, the assumption that the mechanical properties of the polymeric scaffold could be described by a neo-Hookean behavior [36]. We thus developed a separate computational model (Matlab program) to model the mechanics of our polymer scaffold over the course of its degradation, guided by neo-Hookean models in the literature [31, 32], and verified its implementation via numerical simulations. However, because this incompressible material model failed to describe our initial set of experimental data on polymer degradation (**Figure 3**), we were not able to confirm prior assumptions by others on polymeric scaffold physical properties – i.e., incompressibility (volume does not change when material is subjected to stress) and isotropy (material properties are uniform in all directions).
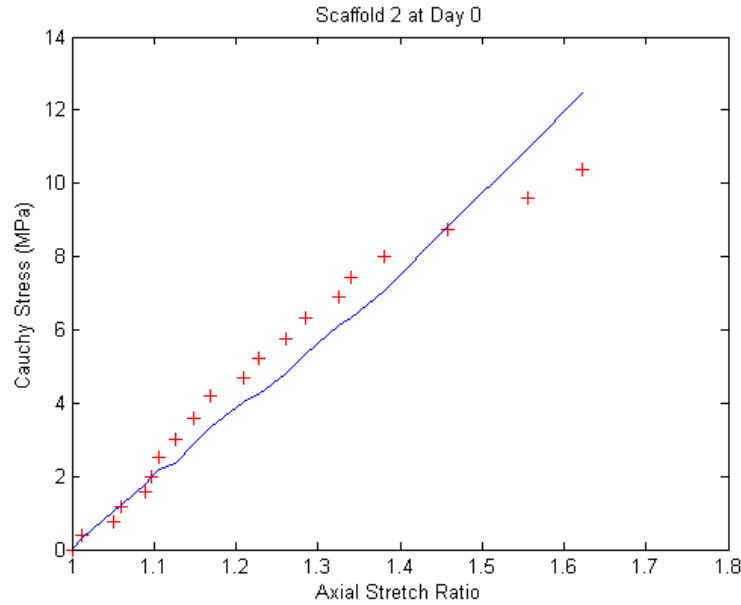
Figure 3: *Pilot result predictions by our initial neo-Hookean model (blue line) were not consistent with experimental data on scaffold degradation (red +'s).*

It is possible that the scaffold exhibits an evolving compressible behavior due to changes in porosity, or that the original scaffold testing protocol and data analysis needed to be refined. Additionally, the simple sigmoidal decay that we assumed for the scaffold may not accurately reflect the time-course of degradation. These assumptions needed to be re-evaluated and the constitutive relations modified accordingly if the scaffold is compressible (e.g., Blatz-Ko).

As of yet, there exists insufficient experimental data to confirm the key assumptions about scaffold physical properties in our computational model of *in vivo* TEVG development. Likewise, we know little about the degradation profile of our polymeric scaffold. *In vitro* degradation studies of PGA scaffolds can provide a reasonable approximation of PGA degradation *in vivo*. This approach circumvents the problem of

separating partially degraded scaffold from regenerated tissue, and the data obtained for PGA scaffolds in buffer have been proven to match the calculation of polymer degradation in cell-PGA constructs [37]. Freed and colleagues seeded nonwoven PGA meshes with chondrocytes and accurately predicted the total cell-polymer construct mass by summing the products of cellular accumulation (cells, glycosaminoglycans, and collagen measured in cell-polymer constructs) with scaffold degradation (the mass of the remaining PGA measured from their *in vitro* degradation study) [37]. Also, PGA fibers will degrade similarly in neutral phosphate-buffered solution (PBS) at 37°C as they would *in vivo* in extracellular fluid; bulk hydrolysis is the main degradation mechanism for PGA fibers, meaning that the fibers erode both inside and on the surface, independent of surface-to-volume ratio [38]. Herein, we report the effects of *in vitro* hydrolytic degradation on the mechanical behavior of cylindrical scaffolds composed from nonwoven PGA fibrous felt, as well as a novel method for assessing the compressibility and real-time changes in scaffold dimensions during mechanical testing.

Hypothesis

There is a well-established connection between intimal hyperplasia and synthetic vascular grafts that alter the mechanical stresses experienced by the host vessel [39]. This phenomenon appears to result from changes in gene expression that vascular cells undergo in response to perturbations in mechanical stimuli – for example, biomechanical effects of compliance mismatch between graft and native vasculature [40, 41]. We *hypothesize* that synthetic cells populating TEVGs produce extracellular matrix in a predictable manner to

promote mechanical homeostasis throughout the remodeling process, and that by matching the evolving compliance of the graft with that of the host vessel, we may decrease the incidence of TEVG stenosis. We *hypothesize* further that inflammation mediates the early maturation phase of TEVGs into fully functional vessels *in vivo*, which involves both innate and adaptive components of the immune system. Monocytes and macrophages appear to initiate an inflammatory cascade that recruits cells from adjacent native vessel and forms neotissue at the graft site, analogous to postnatal neovascularization [11, 12]. T cells, the main actors in adaptive immunity, also influence postnatal neovascularization [42]. We **hypothesize** that the changing mechanical and material behavior of the degrading scaffold will cause corresponding changes in ECM production by immune and vascular cells, ultimately reflected by the TEVG's mechanical behavior.

Our **overall goal** is to construct a validated, predictive computational model that enables time-efficient parameter sensitivity studies that identify ways to improve the functional compatibility between the graft and host vessel, thus expediting the development of advanced TEVGs by rational design. Toward that end, the **purpose** of this study is threefold: to evaluate the assumptions about scaffold physical properties in our first-generation growth and remodeling computational model, to collect the experimental data needed to inform the next generation of computational models, and to develop and validate a novel method of measuring real-time changes in scaffold geometry – both inside and on the surface of the sample – during mechanical testing.

Specific Aims

- Evaluate the evolving mechanical properties of PGA scaffolds undergoing *in vitro* hydrolytic degradation.

- Characterize the compressibility of the polymer scaffold.

Methods

Scaffold fabrication

Tubular TEVG scaffolds were constructed by Cameron Best (Nationwide Children's Hospital, Columbus, OH) from sheets of nonwoven poly(glycolic acid) (PGA; Concordia Fibers, Coventry, RI) that were wrapped around a 21G needle, placed in a 20 μm-diameter mold, and sealed with a 50:50 copolymer of ε-poly(caprolactone) and L-poly(lactide) (P[PC/LA]; Absorbable Polymers International, Birmingham, AL). Scaffolds ranged from 3 to 3.5 mm long with an inner diameter of ~700 to 800 μm and a wall thickness of ~290 to ~360 μm. Specifications given by Concordia Fibers for the nonwoven PGA fiber felt sheets include: polymer specific gravity 1.5 - 1.7 g/cm^3; felt density 150 mgr / cm^3; PGA fiber diameter ~14 - 16 μm; felt thickness ~0.3 mm.

Degradation studies

Dry scaffolds were weighed to record their initial masses and incubated at 37 ºC in micro-tubes containing 1 mL of phosphate buffered solution at pH 7.03 (PBS; Gibco,

Grand Island, NY). Every week for 10 weeks, the pH of the medium was measured (Accumet AP71 pH/mV/C meter, Fisher Scientific, Waltham, MA) and PBS was replaced to maintain pH between 7.0 and 7.1 inside the micro-tubes, replicating how blood flow removes degradation byproducts and prevents the micro-environment pH from becoming overly acidic. Change in pH (ΔpH) per week was calculated as:

$$\Delta pH = pH - 7.0$$

where pH is the instantaneous pH at time of measurement.

One set of scaffolds (n = 5) was removed at timed intervals of 5 days for over 40 days, and then at intervals of 7 days for 4 more weeks. Scaffolds were dried by lyophilization and re-weighed to calculate the dry mass ratio,

$$Dry\ mass\ ratio = \frac{M}{M_0}$$

where the subscript 0 denotes a specimen-specific initial value.

Cannula preparation

Cannula used for mounting the scaffolds during testing were prepared by crimping and roughing the ends of 21G needles with sand-paper to prevent slippage; the scaffolds were then mounted and tightly secured to the cannula with 7-O silk tie suture. India ink was used to mark the scaffold at least one-diameter length away from each cannulated end so that the effects of tying (e.g., axial variations in strain) are minimized according to Saint-Venant's principle, which suggests that any state of stress with an equivalent resultant force

and couple at the end will not alter the expected stress or strain at distances remote from the point where load is applied (i.e., tied ends of scaffold) [43].

Mechanical testing

PGA scaffolds were removed from the incubator and subjected to uniaxial tensile loading every 5 days over 4 weeks (n = 5 at every time point). Mechanical testing occurred under semi-biomimetic conditions – in PBS at 25° C – since polymers are viscoelastic and exhibit time-dependent behavior that will change with temperature, loading rate, and wet-versus-dry state [44-46]. There is a clear decrease over time in mechanical properties from dry to wet states once polyester scaffolds have been wetted in PBS for 0.5 hours, but their properties remain stable and do not diminish significantly from 0.5 to 24 hours after being hydrated [47]. Therefore, the PGA scaffolds were immersed in PBS for 30 minutes before testing.

Due to the porous nature of the PGA felt, the scaffolds could not hold pressure in our bi-axial mechanical testing system; hence, a custom mechanical testing system was designed in SolidWorks CAD software (Dassault Systèmes S.A., Vélizy-Villacoublay, France) and built to incorporate a VMS-001 micro-camera (Veho, Hampshire, United Kingdom) and ThorLabs Callisto OCT system (Thorlabs, Inc., Newton, NJ) (**Figure 4A**). The specimen was immersed in a fluid bath containing PBS, with one cannula fixed to the bath wall and the other attached to weights via a pulley system (**Figure 4B**).

Quasi-static loads were imposed in increasing increments of 10g until the scaffold reached approximately *in vivo* stretch ($\lambda \sim 1.2$ for venous TEVGs at 6 weeks [22]); if the

scaffold became fragile due to degradation, it was loaded in 2g increments until it experienced plastic deformation. After five cycles of tensile testing – three of which are preconditioning, following the mechanical testing protocol of Klouda et al [46] – one intact scaffold from each time-point group underwent an additional cycle in which the inner and outer radii at each loading step were measured by OCT. For this sixth cycle, the scaffold was immersed in glycerol rather than PBS to accommodate the limitations of OCT imaging (discussed further below). To eliminate air trapped inside the pores, scaffolds were first evacuated of all air and then immersed in glycerol while maintaining vacuum.
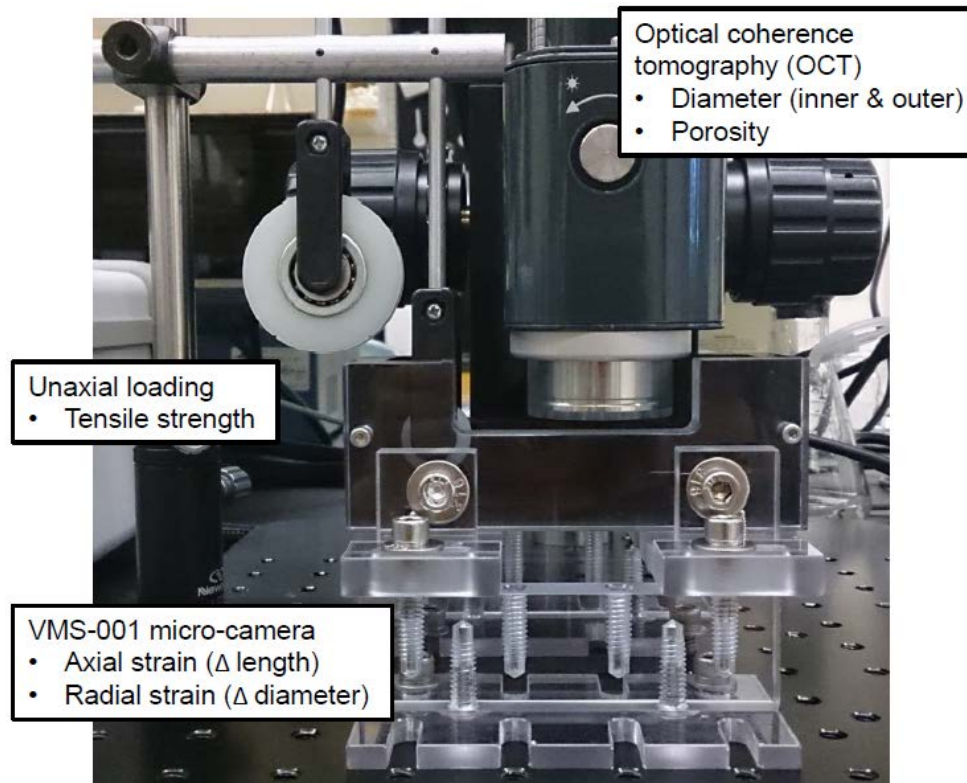

Figure 4: (A) Mechanical testing set-up. Real-time changes in scaffold dimensions are captured by the VMS-001 micro-camera and ThorLabs Callisto optical coherence tomography (OCT) system during uniaxial tensile testing.
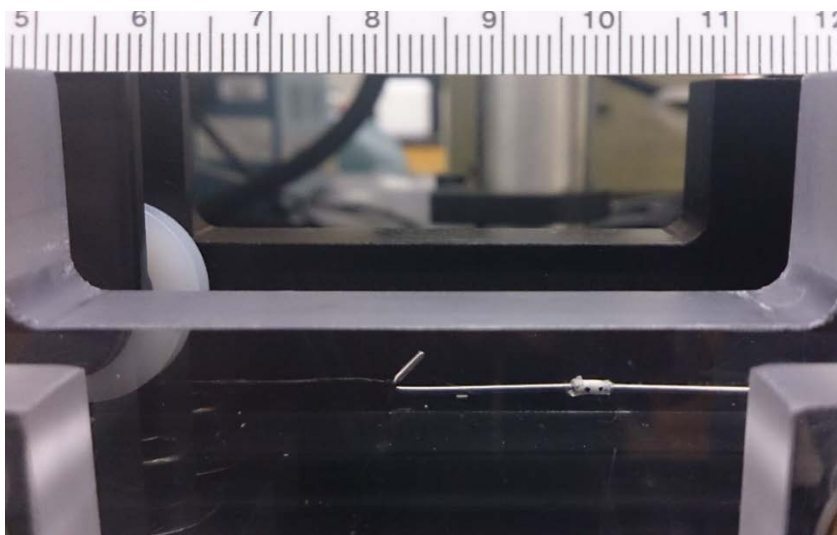
Figure 4*: (**B**) During uniaxial tensile testing, the scaffold is immersed in PBS at room temperature (25°C) inside the fluid chamber. When visualizing the scaffold under OCT, the chamber is filled with glycerol and the air within the scaffold evacuated.*

Imaging PGA scaffolds with OCT

Optical coherence tomography (OCT), similar in concept to ultrasound, uses beams of infra-red light to image cross-sectional slices of a sample and build 3D reconstructions. Unlike scanning electron microscopy, it can visualize changes in real-time on the microscopic scale and does not destroy the sample [48]. However, certain technical challenges initially limited its ability to image our PGA/PCL scaffolds: (1) the Callisto OCT system cannot visualize pore sizes smaller than 7 μm (its maximum resolution); (2) refractive index mismatch between PGA and PBS necessitated the search for a superior imaging solvent; and (3) complex pore geometry trapped air inside the scaffold, compounding the index mismatch, scattering light, and further worsening image quality

(**Figure 5**). Pure glycerol proved to be the most suitable, cost-effective imaging solvent after experimenting with PBS, ethanol, and water in various ratios. Glycerol has a refractive index (1.47) similar to that of PGA (1.45 – 1.51), and it is a safe solvent for OCT imaging of skin and cornea *in vivo* [49].
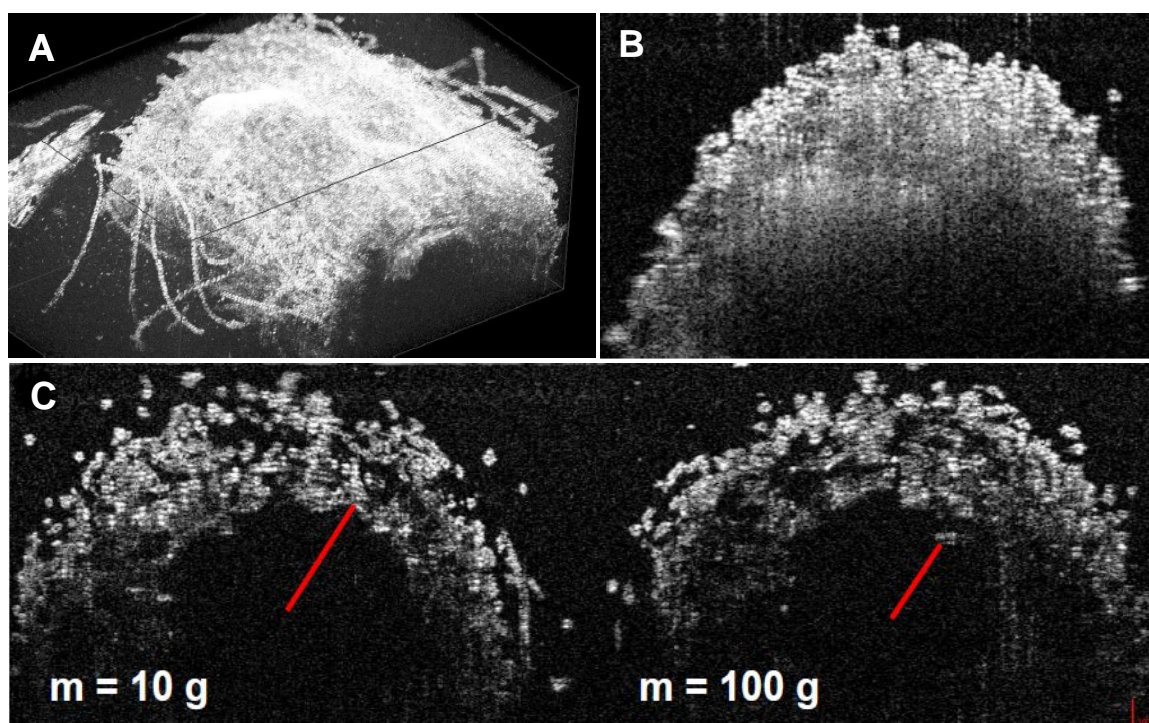
*Figure 5: (**A**) OCT uses infrared light to capture cross-sectional slices and build 3D reconstructions. (**B**) Refractive index mismatch and complex pores that trap air make scaffolds difficult to image with OCT in liquids with low refractive index (e.g., water, PBS, or ethanol). (**C**) Placing scaffolds under vacuum to evacuate air from the pores, followed by immersion in glycerol, vastly improves image quality. Note that the decrease in inner radius is visible as the scaffold is loaded from 10g to 100g.*

The reverse order – complete immersion in fluid, followed by de-gassing – had less of an effect, possibly because this adds another air-fluid interface and thereby increases the capillary pressure that the vacuum must generate. Our procedure requires one outlet for air and one inlet for glycerol; most commercial vacuum chambers contain only one port, however; thus we built a custom vacuum chamber with two ports. Pilot studies did not show a significant difference between the mechanical behavior of scaffolds in glycerol or PBS (**Figure 6**) and no significant difference in thickness before and after immersion (**Figure 7**), making glycerol an acceptable solvent for imaging the scaffold under OCT during tensile tests.
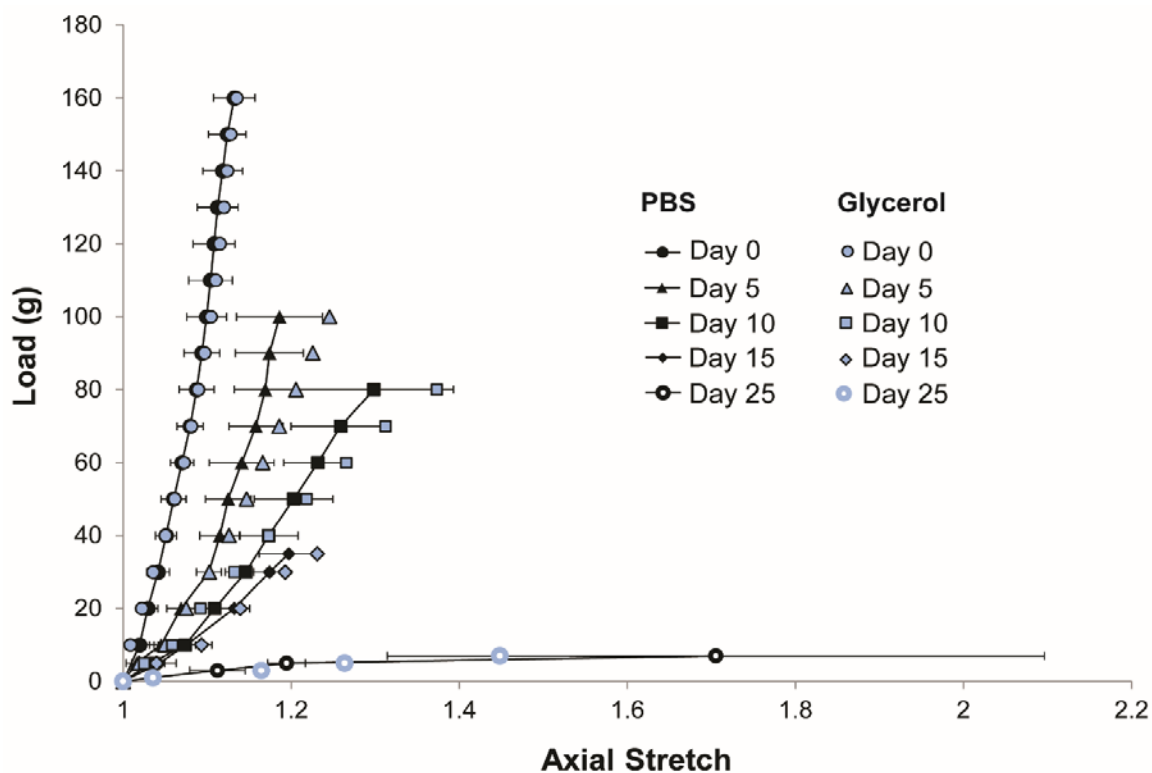
Figure 6: *There is no significant difference in mechanical behavior between scaffolds immersed in glycerol or in PBS (mean ± SD).*
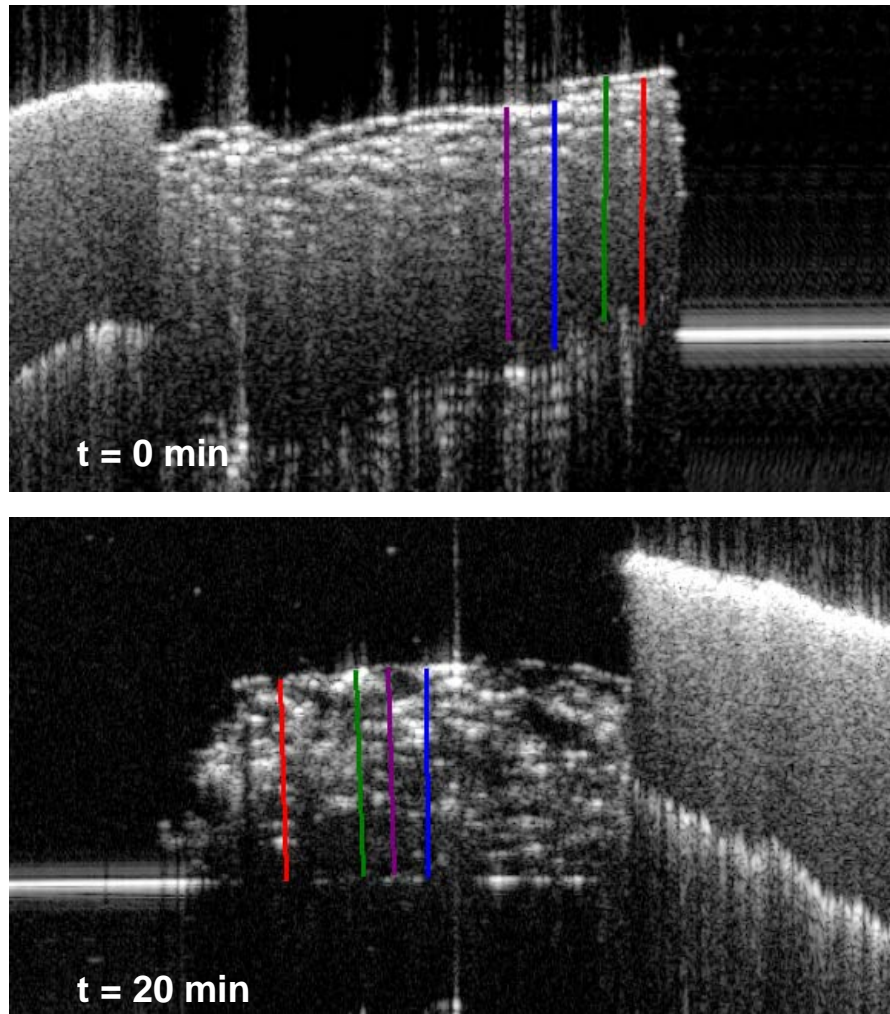
Figure 7*: No significant swelling of the PGA nonwoven fiber felt is visible on OCT before and after immersion in glycerol for 20 minutes (277.4 um ± 7.97 vs. 261.9 um ± 4.19, p < 0.05).*

Optical strain and volume analysis

The VMS-001 micro-camera and the Callisto OCT acquired real-time images at each loading step. ImageJ software (National Institutes of Health, Bethesda, MD) was used

to quantify the scaffold thickness from OCT images, the outer diameter from micro-camera photos, and the length from the distances between India ink marks.

To quantify the mechanical properties of the scaffold, we needed to compute the applied axial stress and resulting extensional strain. Stress is a measure of applied force acting over a cross-sectional area; strain is a non-dimension measure of the change in length. The force (F) applied to the scaffold during uniaxial testing was computed from the applied mass (m), in grams, multiplied by the gravitational constant g times a correction factor (c) that accounted for the friction within the pulleys used in the uniaxial tension tests. That is, $F = mg * c$. To find this correction factor, we used Hooke's law for a metallic calibration spring, which states that force (F) is proportional by a spring stiffness (k) to extension (x) of a spring: $F = kx$. The correction factor (c) was the original stiffness (k_0) for a metal spring (loaded only with weights) divided by the altered spring stiffness (k_1) (the spring was loaded in the pulley system):

$$c = \frac{k_0}{k_1} = \frac{37.68}{34.019} = 1.1076$$

The extensional strain experienced by the scaffold is determined easily from the axial stretch (λ), which is calculated as the ratio between the current length and the original unloaded length:

$$\lambda = \frac{L}{L_0}$$

The volume of the polymer at each load was estimated based on the cross-sectional area at the midpoint of each scaffold and the length between the two markings:

$$V = L\left(\pi(R^2 - r^2)\right)$$

where R and r denote outer and inner radii, respectively.

Finally, engineering stress (σ_e) and strain (ε_e) were based on the original cross-sectional area (A_0) and unloaded length (L_0) of the cylindrical scaffold:

$$\sigma_e = \frac{F}{A_0}$$

$$\varepsilon_e = \frac{\Delta L}{L_0}$$

where $\Delta L = L - L_0$. Alternatively, true stress (σ_t) and strain (ε_t) were calculated using the instantaneous cross-sectional area (A) at the time of loading and the natural logarithm of instantaneous axial stretch (i.e., the instantaneous length of the specimen, L, divided by the initial length, L_0).

$$\sigma_t = \frac{F}{A}$$

$$\varepsilon_t = \ln\frac{L}{L_0}$$

Young's modulus (E) was the slope at the linear portion of the engineering stress-strain curve in the 5-30% strain range:

$$E = \frac{\sigma}{\varepsilon}$$

Statistical analysis

Stress-strain curves were smoothed with a moving average filter, normalized by dividing all length measurements by the minimum length, and presented as mean ± standard deviation (SD). All other data were represented as mean ± SD. All other comparisons between groups were performed using a Student's t-test. P-values <0.05 were considered statistically significant.

Results

Mass loss and pH change during scaffold degradation

The degradation of nonwoven PGA fiber scaffolds in neutral PBS at 37°C passed through two stages of first-order decay (**Figure 8** and **Table 2**). The first 50 percent of PGA mass decreased from 5 to 40 days (~1 to 6 weeks) with a rate constant of 0.175 wk^{-1}, after which the mass degraded with a rate constant of 0.091 wk^{-1}. After 10 weeks *in vitro*, the PGA had degraded to less than 30 percent of its initial mass, similar to results reported by Freed et al. [37].

The pH curve is represented as the weekly change in pH from pH 7.0 (**Figure 8** and **Table 3**). Acidic degradation byproducts may cause autocatalysis and thereby hasten the rate of polymer degradation, so in an effort to mimic the *in vivo* removal of glycolic acid byproducts from the TEVG by blood flow, the PBS was replaced weekly to maintain a pH of 7.0-7.1 around the scaffolds [26]. The highest change in pH occurred between 3 and 6 weeks, coinciding with the first half of PGA mass decay. Thereafter, there is a drastic drop

in pH change, just as PGA mass degradation enters its slower period of degradation. This correlation shows how degradation depends on polymer mass; when only 50 percent of the scaffold remains, the rate of degradation decreases, and as a result, less acidic byproducts are produced.
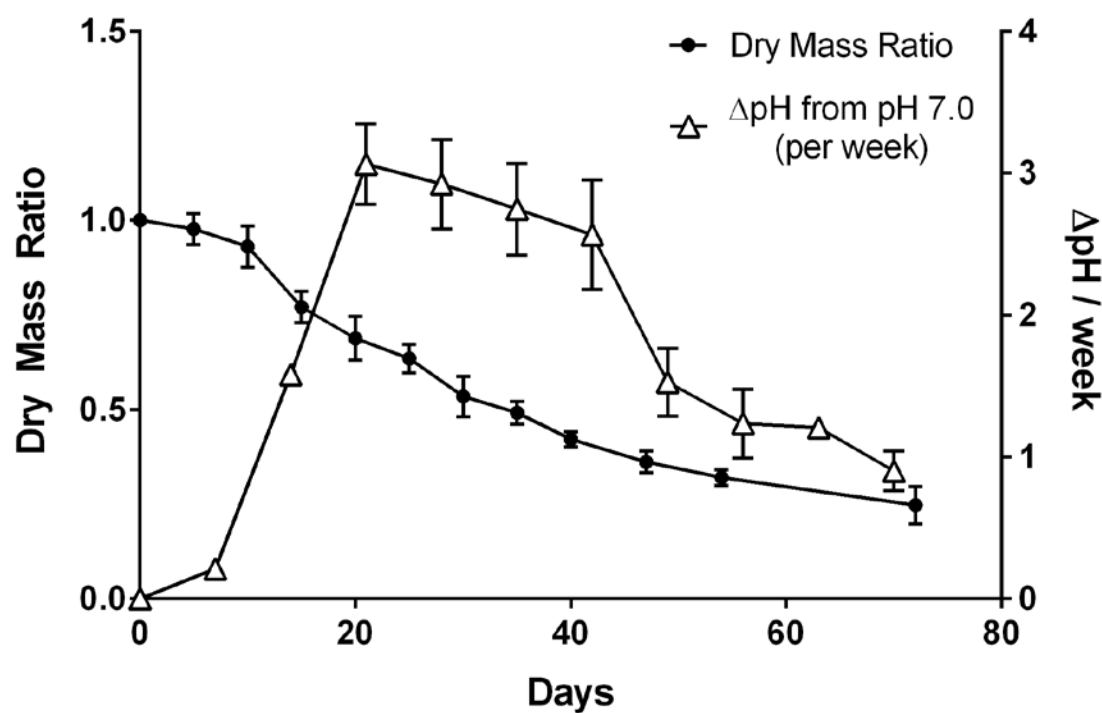
Figure 8: Dry mass ratio (left axis, mean ± SD) and change in pH per week (right axis, mean ± SD). PGA mass follows two stages of first-order decay. The half-life of PGA degradation is 5-6 weeks, coinciding with a decrease in the rate of change in pH. Change of pH (ΔpH) per week is calculated with respect to pH 7.0 because the PBS was replaced weekly to return the medium to neutral pH (i.e., minimize autocatalysis). Thus, ΔpH of 3 at 21 days means that the production of acidic degradation byproducts from PGA scaffolds occurred the fastest at week 3 of hydrolysis.

Table 2: *Dry mass ratio versus degradation time (mean ± SD).*

Days	Dry Mass Ratio	SD
0	1.000	0.000
5	0.989	0.015
10	0.918	0.092
15	0.757	0.075
20	0.663	0.073
25	0.594	0.031
30	0.525	0.057
35	0.496	0.083
40	0.426	0.043
47	0.373	0.047
54	0.331	0.009
72	0.278	0.063

Table 3: *Change in pH from neutral pH per week (mean ± SD). PBS in the micro-tubes was changed every week to keep the medium surrounding the scaffolds at pH 7.0.*

Days	ΔpH (from neutral pH)	SD
0	0.00	0.05
7	0.21	0.03
14	1.58	0.28
21	3.06	0.32
28	2.92	0.32
35	2.75	0.39
42	2.56	0.24
49	1.53	0.24
56	1.24	0.02
63	1.21	0.14
70	0.90	0.00

Decreasing modulus and increasing variability of scaffold behavior

As the PGA scaffolds degraded, the Young's modulus decreased and the mechanical behavior of the scaffolds also became increasingly variable, as evidenced by the widening of the standard deviation error bars (**Figures 9 – 11** and **Table 4**). There appeared to be three subsets of mechanical behavior: from 0 to 5 days, the scaffolds were stiffest as expected; on days 10 and 15, the modulus decreased with a concomitant drop in yield strength, losing nearly half by day 15; and by days 20 and 25, the scaffolds had lost more than 90 percent of their mechanical strength and exhibited plastic deformation. Prior to day 15, the scaffolds were fairly robust. On day 15 and afterwards, however, the fragile scaffold required careful handling; it would separate into fiber "fragments" when loaded or sometimes the proximal and distal fragments would shift under tension, whereas unconnected fibers in the middle appeared to not move. These variable behaviors increased the difficulty of mechanical testing because the load was not distributed homogenously throughout the entire scaffold structure, and the tracking markers had to be precisely placed on fragments that moved. The fragmentation is most likely because the scaffold is composed of non-woven PGA fibers that are matted together, but not necessarily all linked physically. In the day 20 group, it also became apparent that the seam line is a weak point; scaffolds were more degraded and failed more often at the seam line.

Hysteresis – the energy dissipated by the material while loaded and unloaded - grows larger on the first testing cycle (preload) as the scaffold is degraded from 0 to 10 days, possibly because hydrolysis has broken enough ester bonds to render the PGA more compliant (**Figure 12).** Additionally, the scaffolds do not return to their original

configuration after unloading. There are no hysteresis curves shown for the time points after day 10 because the scaffolds have weakened and plastically deform instead.
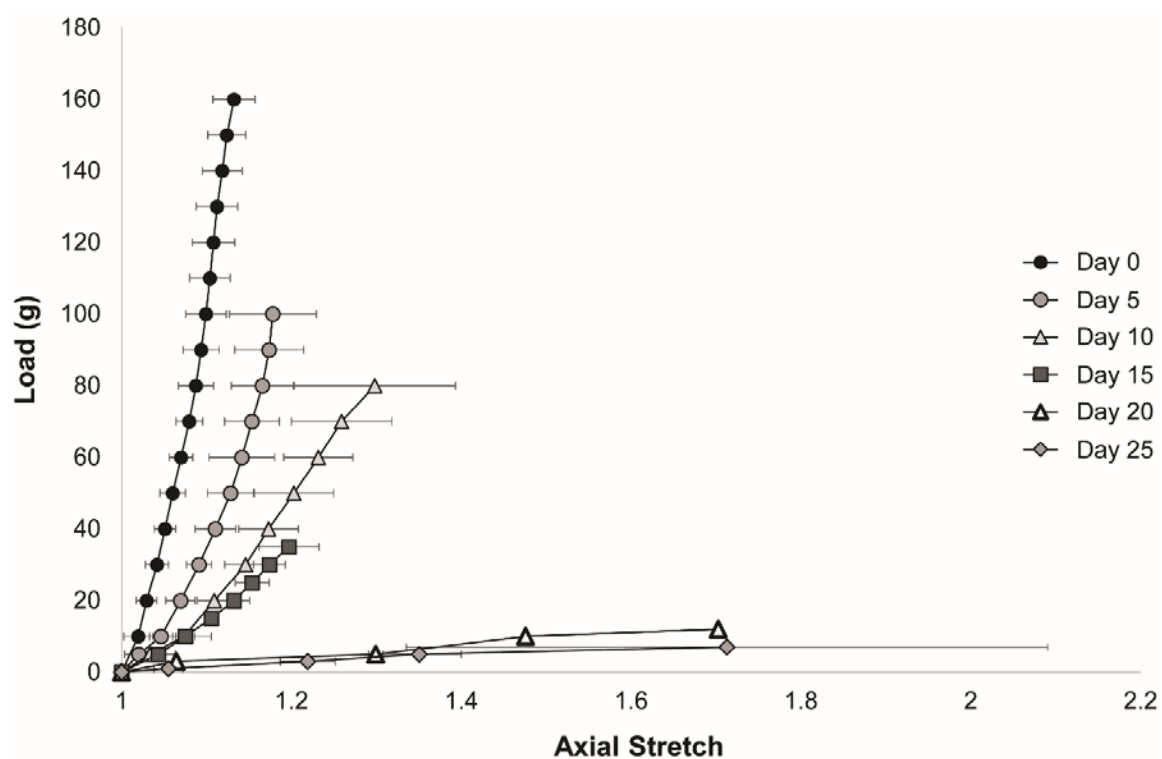

Figure 9: Load vs. axial deformation. With increasing degradation time, Young's modulus decreases, i.e., the scaffolds become less stiff, and the mechanical behavior of the scaffolds becomes increasingly variable, as evidenced by the widening standard deviation error bars.

Days	Young's modulus (MPa)	Correlation coefficient
0	6.449	0.997
5	5.346	0.991
10	2.571	0.999
15	2.014	0.997
25	0.120	0.998

Table 4: Young's modulus of PGA scaffolds decreases over time of hydrolysis.
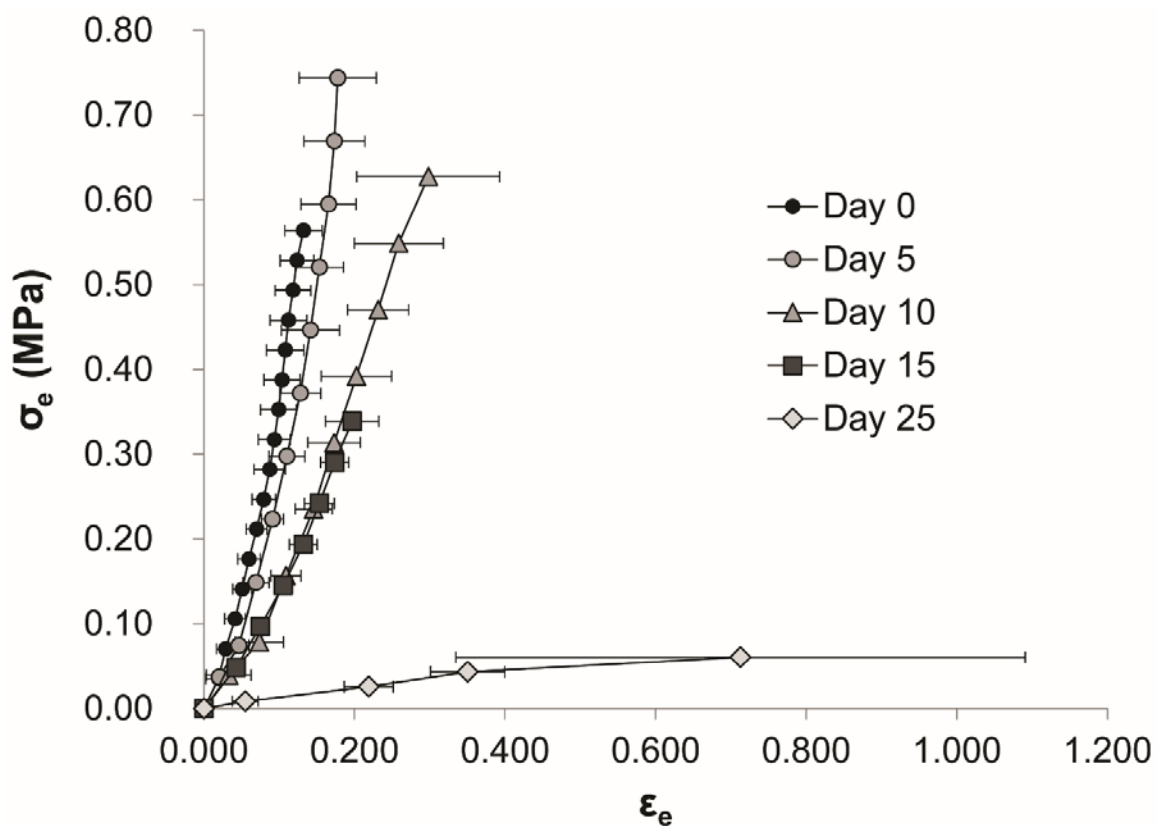
*Figure 10:* Engineering stress vs. strain of PGA scaffolds over degradation time.
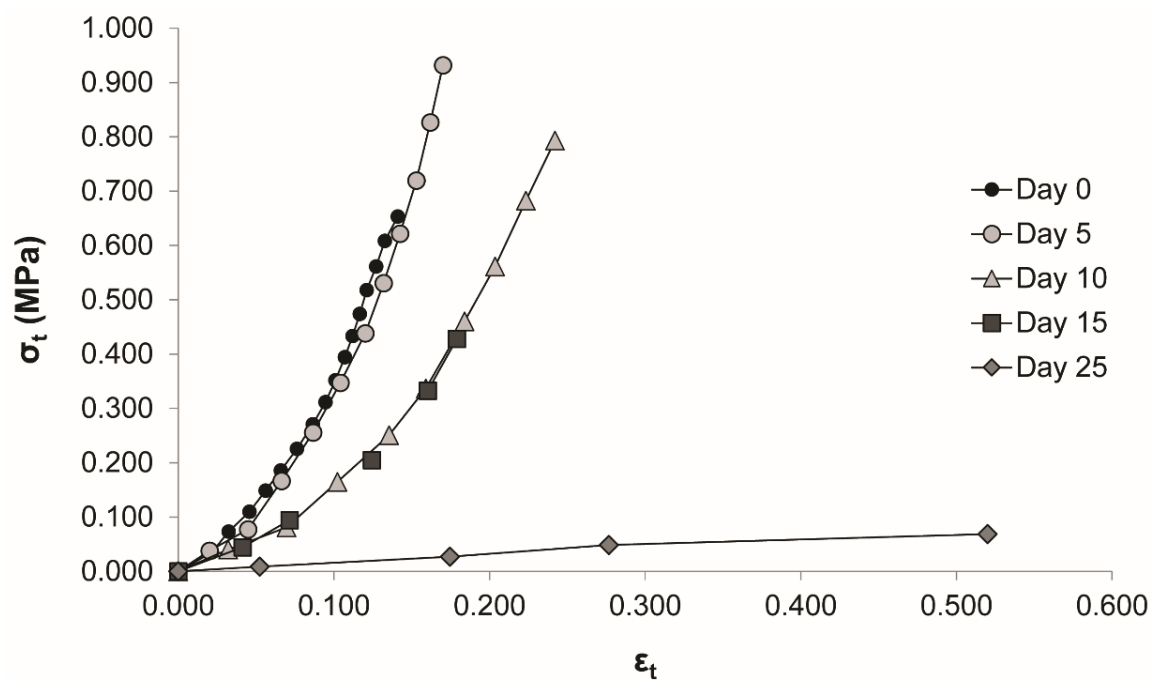
Figure 11: True stress vs. strain of PGA scaffolds over degradation time.

Figure 12: Hysteresis on preload (the first testing) cycle grows larger with time of degradation, possibly because hydrolysis has broken enough ester bonds to render PGA more compliant.
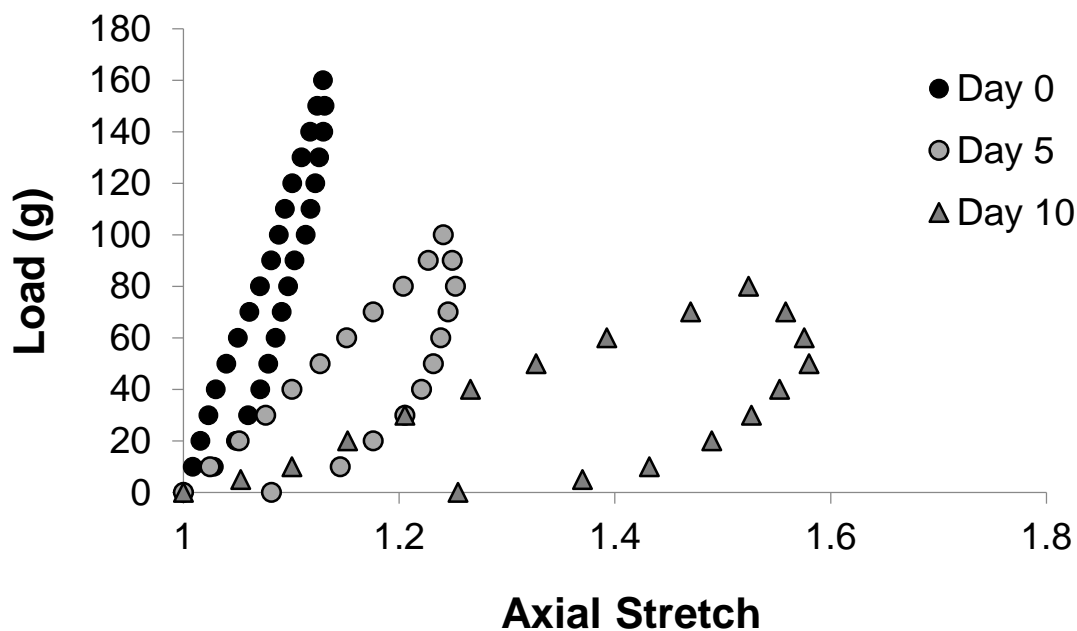
Incompressibility of degrading PGA scaffolds

PGA scaffolds remain relatively incompressible through most of the degradation and their volume stays constant during loading, except at day 25 when the compressibility seems to manifest (**Figure 13**). This transition may be attributed to the fact that the scaffolds are heterogeneously fragmented by this time; the load will not be transmitted evenly throughout the material, hence an axial extensional strain will not necessarily cause a transverse compressive strain (i.e., true Poisson effect), and the outer diameter of the fragmented scaffold does not change accordingly. Scaffold volume and cross-sectional area

do   decrease   over   time,   however,   as   expected   (**Figure   14**).
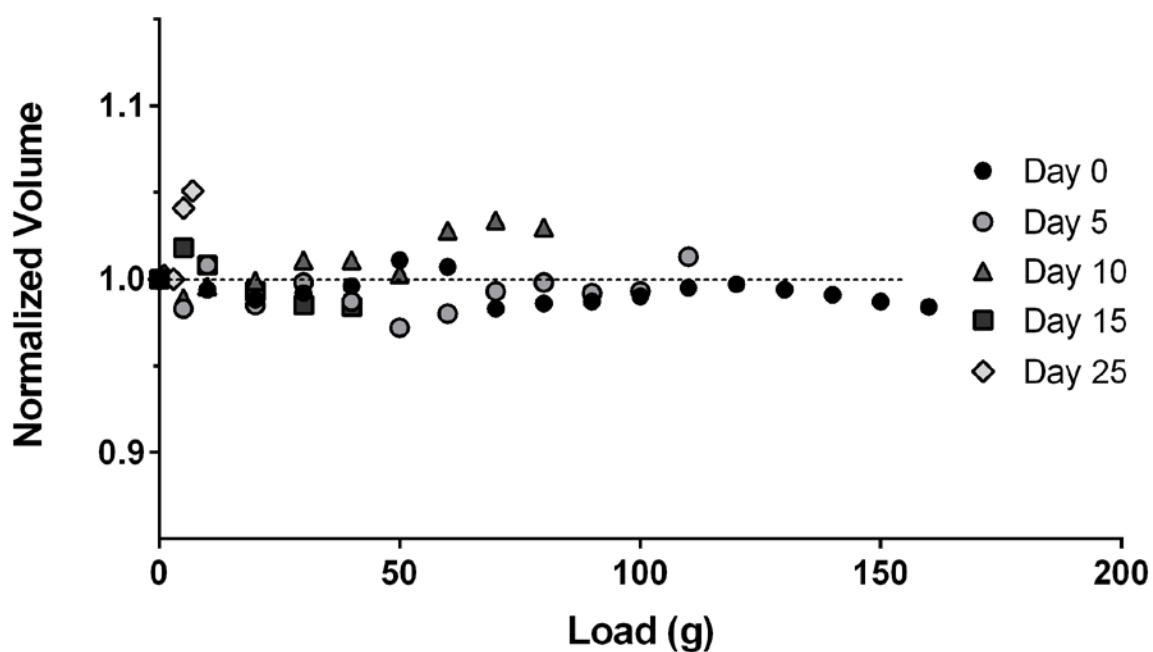
Figure 14: *PGA scaffolds remain relatively incompressible through most of degradation, i.e., volume stays constant during loading, except at day 25 when the polymer scaffold's volume seems to increase during loading. This may be attributed to the fact that the scaffolds are heterogeneously fragmented and the load is not transmitted evenly throughout the material. Hence, a positive tensile strain will not contribute a negative compressive strain in the lateral direction, and the outer diameter of the fragmented scaffold does not change appropriately.*
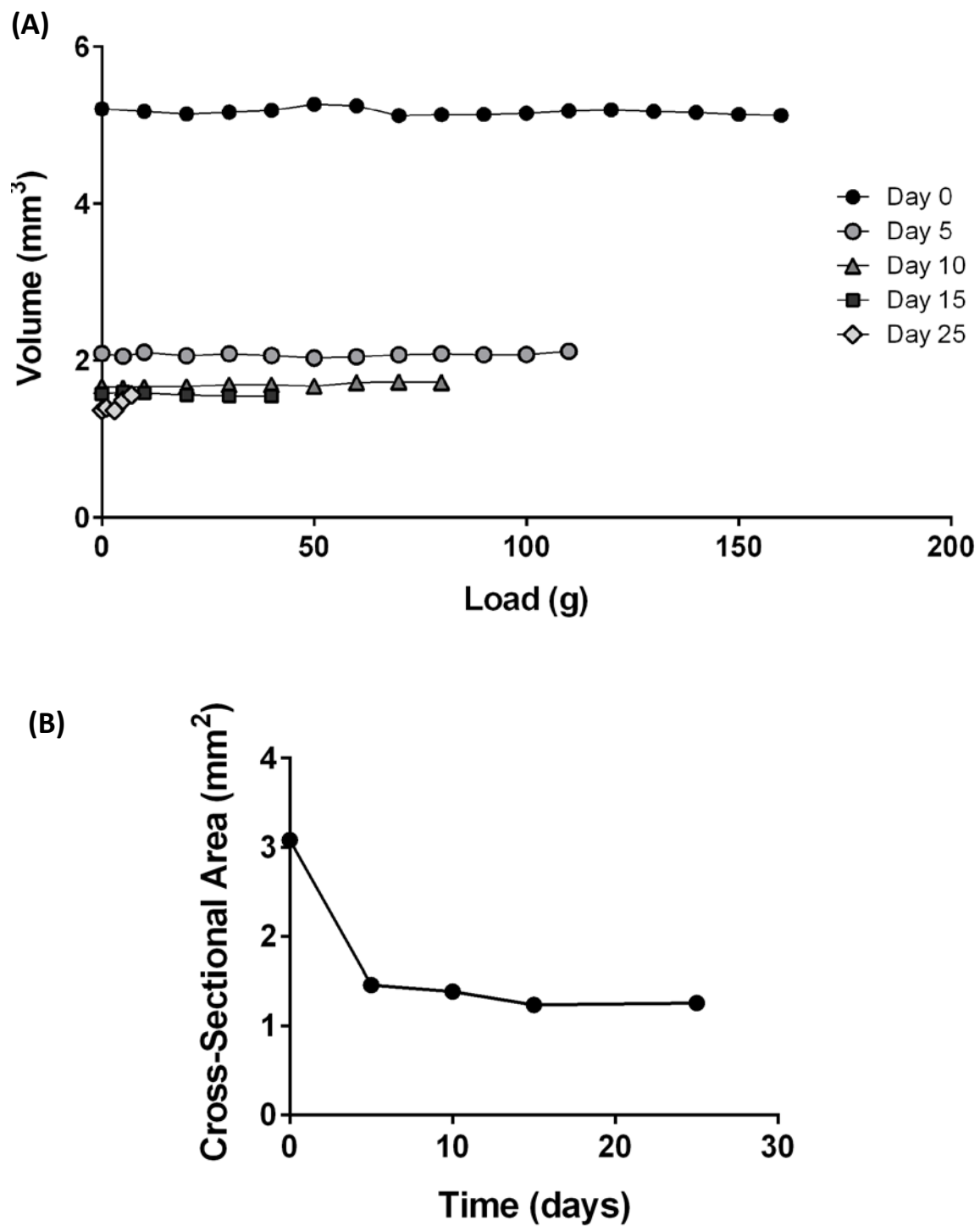
Figure 14: *More than half of the scaffold volume (**A**) and cross-sectional area (**B**) is lost by 5 days of hydrolytic degradation.*

Discussion

Herein we report the effects of *in vitro* hydrolytic degradation on the mechanical behavior of cylindrical tissue engineering scaffolds composed primarily of a nonwoven PGA fibrous felt, as well as a novel method for assessing the compressibility and real-time changes in scaffold dimensions during uniaxial mechanical testing. As an aliphatic (open chain, non-aromatic) polyester, PGA degrades in an aqueous environment primarily through bulk erosion; hydrolytic attack cleaves the ester bond backbone, causing random chain scission on both the surface and the inside of PGA fibers [20, 50]. Autocatalysis can occur inside the core of the material due to acidic degradation byproducts trapped within the substrate. By attempting to control this effect and keep the medium at a neutral pH, we collected and analysed experimental data that correlate changes in pH – an important determinant of degradation rate – with PGA mass loss in the two stages of a first-order exponential decay. This study found a PGA *in vitro* half-life of 6 weeks, whereas Naito and colleagues report that PGA lost half its volume *in vivo* in just 2 weeks [22]. Proteolytic activity as part of the *in vivo* foreign body response could be responsible for this discrepancy, and there exists evidence that various enzymes like carboxypeptidase A can increase the rate of PGA hydrolysis [20].

Scaffold degradation adds another layer of complexity to computational modeling. Intuitively, the scaffold's changing mechanical and material behavior will drive corresponding adaptations in the immune and vascular cells responsible for neovessel development. Importantly, the rate of tissue regeneration should match polymer degradation. Improperly timed degradation has poor consequences for the transition from

acute inflammation-mediated to the mechano-biological dominated production of matrix, as shown by the highly stiff poly(lactic acid), that is PLA, aortic TEVGs which showed signs of chronic inflammation secondary to inadequate *in vivo* degradation of PLA [27]. Khosravi and colleagues discovered that phenotypic diversity manifested via two sub-groups of 2 year old grafts, characterized with two different compliances, despite all procedures being the same, and that increased variability of experimental data at 24 weeks and 2 years could be simulated by changing two model parameters – mechano-mediated collagen material properties and the half-life of collagen produced during inflammatory period [2]. Perhaps another contributing factor to the increased variability of TEVG data at two years could be the increasing heterogeneity of scaffold behavior due to degradation; as the polymer scaffold degrades over time, its loss of structural integrity will influence its mechanical contribution and hence its overall effect on the remodeling process, including collagen deposition.

We have taken a step forward in characterizing the effects of hydrolytic degradation on the mechano-physical properties of venous polymeric scaffolds, and our results show that the PGA scaffolds are indeed incompressible up until 25 days of degradation. However, more complete data are necessary to evaluate assumptions in our first-generation model and to illustrate clearly the evolving mechanical behavior of polymeric scaffolds. The degrading PGA scaffolds do not return to their original configuration after pre-loading, and it is not clear what is giving rise to such complex physical behavior. The reason could be on a molecular level – breaking of secondary bonds, internal sliding and friction of macromolecular polymer chains, physical entanglements of fibers, or the large-scale fragmentation of the scaffold into non-woven fiber segments after unloading [44]. Since

the scaffold is a blend of polymers – PGA coated with PCL - it is also a candidate for the Mullins effect, which is an irreversible softening of the stress-strain behavior whenever the load increases beyond its prior maximum value [44]. No matter the cause, the polymer behaves in a complex manner as it evolves *in vitro*, and this dissipative, non-elastic process must be taken into account in any computational model.

There clearly remains a pressing need for further investigations of scaffold properties and their interactions with matrix production by immune and vascular cells. The processes underlying vascular growth and remodeling must be further elucidated in order to develop therapeutic interventions against graft stenosis or dilation, and to build a computational model that accurately captures how engineered tissues mature into neovessels.

References

1. Shinoka, T. and Breuer, C. *Tissue-Engineered Blood Vessels in Pediatric Cardiac Surgery.* The Yale Journal of Biology and Medicine. 2008. **81**(4):161-166.

2. Khosravi, R., Miller, K.S., Best, C.A., Shih, Y.C., Lee, Y.U., et al. *Biomechanical Diversity Despite Mechanobiological Stability in Tissue Engineered Vascular Grafts Two Years Post-Implantation.* Tissue Eng Part A. 2015.

3. Shin'oka, T., Imai, Y. and Ikada, Y. *Transplantation of a tissue-engineered pulmonary artery.* N Engl J Med. 2001. **344**(7):532-3.

4. Hoffman, J.I. and Kaplan, S. *The incidence of congenital heart disease.* J Am Coll Cardiol. 2002. **39**(12):1890-900.

5. Boulet SL, G.S., Riehle-Colarusso T, Correa-Villasenor A. *Health Care Costs of Congenital Heart Defects*. In *Congenital Heart Defects: From Origin to Treatment*. A.C.-V. DF Wyszynski, TP Graham, Editor. 2010. New York City: Oxford University Press. 493-501.

6. Reller, M.D., Strickland, M.J., Riehle-Colarusso, T., Mahle, W.T. and Correa, A. *Prevalence of congenital heart defects in metropolitan Atlanta, 1998-2005.* J Pediatr. 2008. **153**(6):807-13.

7. Oster, M.E., Lee, K.A., Honein, M.A., Riehle-Colarusso, T., Shin, M., et al. *Temporal trends in survival among infants with critical congenital heart defects.* Pediatrics. 2013. **131**(5):e1502-8.

8. Dearani, J.A., Danielson, G.K., Puga, F.J., Schaff, H.V., Warnes, C.W., et al. *Late follow-up of 1095 patients undergoing operation for complex congenital heart disease utilizing pulmonary ventricle to pulmonary artery conduits.* Ann Thorac Surg. 2003. **75**(2):399-410; discussion 410-1.

9. Chan, B.P. and Leong, K.W. *Scaffolding in tissue engineering: general approaches and tissue-specific considerations.* Eur Spine J. 2008. **17**(Suppl 4):467-79.

10. Hibino, N., McGillicuddy, E., Matsumura, G., Ichihara, Y., Naito, Y., et al. *Late-term results of tissue-engineered vascular grafts in humans.* J Thorac Cardiovasc Surg. 2010. **139**(2):431-6, 436.e1-2.

11. Cleary, M.A., Geiger, E., Grady, C., Best, C., Naito, Y., et al. *Vascular tissue engineering: the next generation.* Trends Mol Med. 2012. **18**(7):394-404.

12. Patterson, J.T., Gilliland, T., Maxfield, M.W., Church, S., Naito, Y., et al. *Tissue-engineered vascular grafts for use in the treatment of congenital heart disease: from the bench to the clinic and back again.* Regen Med. 2012. **7**(3):409-19.

13. Anderson, J.M., Rodriguez, A. and Chang, D.T. *Foreign body reaction to biomaterials.* Semin Immunol. 2008. **20**(2):86-100.

14. Brodbeck, W.G., Voskerician, G., Ziats, N.P., Nakayama, Y., Matsuda, T., et al. *In vivo leukocyte cytokine mRNA responses to biomaterials are dependent on surface chemistry.* J Biomed Mater Res A. 2003. **64**(2):320-9.

15. Bartneck, M., Heffels, K.H., Pan, Y., Bovi, M., Zwadlo-Klarwasser, G., et al. *Inducing healing-like human primary macrophage phenotypes by 3D hydrogel coated nanofibres.* Biomaterials. 2012. **33**(16):4136-46.

16. Saino, E., Focarete, M.L., Gualandi, C., Emanuele, E., Cornaglia, A.I., et al. *Effect of electrospun fiber diameter and alignment on macrophage activation and secretion of proinflammatory cytokines and chemokines.* Biomacromolecules. 2011. **12**(5):1900-11.

17. Madden, L.R., Mortisen, D.J., Sussman, E.M., Dupras, S.K., Fugate, J.A., et al. *Proangiogenic scaffolds as functional templates for cardiac tissue engineering.* Proc Natl Acad Sci U S A. 2010. **107**(34):15211-6.

18. Hinz, B. *Matrix mechanics and regulation of the fibroblast phenotype.* Periodontology 2000. 2013. **63**(1):14-28.

19. Tomasek, J.J., Gabbiani, G., Hinz, B., Chaponnier, C. and Brown, R.A. *Myofibroblasts and mechano-regulation of connective tissue remodelling.* Nat Rev Mol Cell Biol. 2002. **3**(5):349-63.

20. ASM-International, *Materials and Coatings for Medical Devices: Cardiovascular*. 2009: ASM International.

21. Wong, W.H. and Mooney, D.J. *Synthesis and Properties of Biodegradable Polymers Used as Synthetic Matrices for Tissue Engineering*. In *Synthetic Biodegradable Polymer Scaffolds*. A. Atala, D. Mooney, J. Vacanti, and R. Langer, Editors. 1997. Boston: Birhauser Basel. 50-82.

22. Naito, Y., Lee, Y.U., Yi, T., Church, S.N., Solomon, D., et al. *Beyond burst pressure: initial evaluation of the natural history of the biaxial mechanical properties of tissue-engineered vascular grafts in the venous circulation using a murine model.* Tissue Eng Part A. 2014. **20**(1-2):346-55.

23. Boontheekul, T., Hill, E.E., Kong, H.J. and Mooney, D.J. *Regulating myoblast phenotype through controlled gel stiffness and degradation.* Tissue Eng. 2007. **13**(7):1431-42.

24. Higgins, S.P., Solan, A.K. and Niklason, L.E. *Effects of polyglycolic acid on porcine smooth muscle cell growth and differentiation.* Journal of Biomedical Materials Research Part A. 2003. **67A**(1):295-302.

25. Sung, H.J., Meredith, C., Johnson, C. and Galis, Z.S. *The effect of scaffold degradation rate on three-dimensional cell growth and angiogenesis.* Biomaterials. 2004. **25**(26):5735-42.

26. Agrawal, C.M., McKinney, J.S., Lanctot, D. and Athanasiou, K.A. *Effects of fluid flow on the in vitro degradation kinetics of biodegradable scaffolds for tissue engineering.* Biomaterials. 2000. **21**(23):2443-52.

27. Udelsman, B.V., Khosravi, R., Miller, K.S., Dean, E.W., Bersi, M.R., et al. *Characterization of evolving biomechanical properties of tissue engineered vascular grafts in the arterial circulation.* J Biomech. 2014. **47**(9):2070-9.

28. Niklason, L.E., Yeh, A.T., Calle, E.A., Bai, Y., Valentín, A., et al. *Enabling tools for engineering collagenous tissues integrating bioreactors, intravital imaging, and biomechanical modeling.* Proceedings of the National Academy of Sciences. 2010. **107**(8):3335-3339.

29. Miller, K.S., Khosravi, R., Breuer, C.K. and Humphrey, J.D. *A hypothesis-driven parametric study of effects of polymeric scaffold properties on tissue engineered neovessel formation.* Acta Biomater. 2015. **11**:283-94.

30. O'Dea, R.D., Osborne, J.M., El Haj, A.J., Byrne, H.M. and Waters, S.L. *The interplay between tissue growth and scaffold degradation in engineered tissue constructs.* J Math Biol. 2013. **67**(5):1199-225.

31. Vieira, A.C., Vieira, J.C., Ferra, J.M., Magalhaes, F.D., Guedes, R.M., et al. *Mechanical study of PLA-PCL fibers during in vitro degradation.* J Mech Behav Biomed Mater. 2011. **4**(3):451-60.

32. Soares, J.S., Moore, J.E., Jr. and Rajagopal, K.R. *Constitutive framework for biodegradable polymers with applications to biodegradable stents.* Asaio j. 2008. **54**(3):295-301.

33.   Roh, J.D., Nelson, G. N., Brennan, M. P., Mirensky, T. L., Yi, T., Hazlett, T., … Breuer, C. K. *Small-diameter biodegradable scaffolds for functional vascular tissue engineering in the mouse model.* Biomaterials. 2008. **29**(10): 1454–1463.

34.   Gleason, R.L., Wilson, E. and Humphrey, J.D. *Biaxial biomechanical adaptations of mouse carotid arteries cultured at altered axial extension.* J Biomech. 2007. **40**(4):766-76.

35.   Lee, Y.U., Naito, Y., Kurobe, H., Breuer, C.K. and Humphrey, J.D. *Biaxial mechanical properties of the inferior vena cava in C57BL/6 and CB-17 SCID/bg mice.* J Biomech. 2013. **46**(13):2277-82.

36.   Miller, K.S., Lee, Y.U., Naito, Y., Breuer, C.K. and Humphrey, J.D. *Computational model of the in vivo development of a tissue engineered vein from an implanted polymeric construct.* J Biomech. 2014. **47**(9):2080-7.

37.   Freed, L.E., Vunjak-Novakovic, G., Biron, R.J., Eagles, D.B., Lesnoy, D.C., et al. *Biodegradable polymer scaffolds for tissue engineering.* Biotechnology (N Y). 1994. **12**(7):689-93.

38.   Gao, J., Niklason, L. and Langer, R. *Surface hydrolysis of poly(glycolic acid) meshes increases the seeding density of vascular smooth muscle cells.* J Biomed Mater Res. 1998. **42**(3):417-24.

39.   Abbott, W.M., Callow, A., Moore, W., Rutherford, R., Veith, F., et al. *Evaluation and performance standards for arterial prostheses.* J Vasc Surg. 1993. **17**(4):746-56.

40.   Humphrey, J.D. *Vascular adaptation and mechanical homeostasis at tissue, cellular, and sub-cellular levels.* Cell Biochem Biophys. 2008. **50**(2):53-78.

41.   Ingber, D.E. *Mechanical control of tissue growth: Function follows form.* Proceedings of the National Academy of Sciences of the United States of America. 2005. **102**(33):11571-11572.

42.   la Sala, A., Pontecorvo, L., Agresta, A., Rosano, G. and Stabile, E. *Regulation of collateral blood vessel development by the innate and adaptive immune system.* Trends Mol Med. 2012. **18**(8):494-501.

43.   Van Ee, C. and Myers, B.S., *Techniques and Applications for Strain Measurements of Skeletal Muscle*, in *Musculoskeletal Models and Techniques*, C.T. Leondes, Editor. 2000, CRC Press.

44.   Wiley, *Properties and Behavior of Polymers*. Vol. 1. 2012, Hoboken, New Jersey: John Wiley & Sons, Inc.

45.   Wu, L., Zhang, J., Jing, D. and Ding, J. *'Wet state' mechanical properties of three-dimensional polyester porous scaffolds.* J Biomed Mater Res A. 2006. **76**(2):264-71.

46.   Klouda, L., Vaz, C.M., Mol, A., Baaijens, F.P. and Bouten, C.V. *Effect of biomimetic conditions on mechanical and structural integrity of PGA/P4HB and electrospun PCL scaffolds.* J Mater Sci Mater Med. 2008. **19**(3):1137-44.

47.   Wu, L., Zhang, J., Jing, D. and Ding, J. *"Wet-state" mechanical properties of three-dimensional polyester porous scaffolds.* J Biomed Mater Res A. 2006. **76**(2):264-71.

48.   Liang, X., Graf, B.W. and Boppart, S.A. *Imaging engineered tissues using structural and functional optical coherence tomography.* J Biophotonics. 2009. **2**(11):643-55.

49.   Wang, R.K. and Tuchin, V.V. *Optical Coherence Tomography: Light Scattering and Imaging Enhancement*. In *Handbook of Coherent-Domain Optical Methods*. 2013. New York: Springer Science+Business Media. 665.

50.   Sanjukta, D. *Synthetic and Natural Degradable Polymeric Biomaterials*. In *Biomaterials Fabrication and Processing Handbook*. P.K. Chu and X. Liu, Editors. 2008. Boca Raton: CRC Press. 457-476.